



**QUEEN'S
UNIVERSITY
BELFAST**

An assessment of wind and wave climate as potential sources of renewable energy in the nearshore Shenzhen coastal zone of the South China Sea

Chen, X., Wang, K., Zhang, Z., Zeng, Y., Zhang, Y., & O'Driscoll, K. (2017). An assessment of wind and wave climate as potential sources of renewable energy in the nearshore Shenzhen coastal zone of the South China Sea. DOI: 10.1016/j.energy.2017.06.043

Published in:
Energy

Document Version:
Peer reviewed version

Queen's University Belfast - Research Portal:
[Link to publication record in Queen's University Belfast Research Portal](#)

Publisher rights

Copyright 2017 Elsevier.

This manuscript is distributed under a Creative Commons Attribution-NonCommercial-NoDerivs License

(<https://creativecommons.org/licenses/by-nc-nd/4.0/>), which permits distribution and reproduction for non-commercial purposes, provided the author and source are cited.

General rights

Copyright for the publications made accessible via the Queen's University Belfast Research Portal is retained by the author(s) and / or other copyright owners and it is a condition of accessing these publications that users recognise and abide by the legal requirements associated with these rights.

Take down policy

The Research Portal is Queen's institutional repository that provides access to Queen's research output. Every effort has been made to ensure that content in the Research Portal does not infringe any person's rights, or applicable UK laws. If you discover content in the Research Portal that you believe breaches copyright or violates any law, please contact openaccess@qub.ac.uk.

An assessment of wind and wave climate as potential sources of renewable energy in the nearshore Shenzhen coastal zone of the South China Sea

Xinping Chen^a, Kaimin Wang^b, Zenghai Zhang^c, Yindong Zeng^d, Yao Zhang^{a,*}, Kieran O'Driscoll^e

^a*National Marine Hazard Mitigation Service of State Oceanic Administration, Beijing 100194, China.*

^b*Shenzhen Marine Monitoring Forecasting Center, Shenzhen 518067, China.*

^c*National Meteorological Center of China Meteorological Administration, Beijing 100081, China.*

^d*Marine Forecasting Center of Fujian Province, Fuzhou 350003, China.*

^e*School of Natural and Built Environment, Queen's University Belfast, Belfast, Northern Ireland, UK.*

Abstract

In this study, nearshore wind and wave climates and their potential as renewable energy sources are evaluated by means of buoy observational data for the Shenzhen coastal region. Six buoys were originally deployed in the region by the city local government of China in 2014, and are located in different areas of the study region, including Dapeng Bay, Daya Bay, Shenzhen Bay. The waters in these areas are relatively shallow, ranging in depth between about 3-22 m. The results show that during 2014-2016, annual mean wind speeds (at 2.5 m above the sea surface) in the region varied between 3.1-4.1 ms^{-1} , leading to wind powers between 37-94 W m^{-2} ; significant wave

*Corresponding author.

Email addresses: xinp.chen@foxmail.com (Xinping Chen),
yaozhang_zhang@126.com (Yao Zhang)

heights were mostly less than 1 m, while wave energy periods were mostly in the range 3–7 s. As a result, wave power was mostly less than 1.0 kW m^{-1} . It is concluded that the potential of wave energy as a renewable resource at the buoy locations was very small. This may be due to the fact that, first, water depth is very shallow, and, secondly, the buoys are located in bays where the sea is somewhat semi-enclosed, all of which are not favourable for the development of wind waves.

Keywords: Wave climate, Wave energy, Shenzhen, Wind climate, Wind energy, the South China Sea

1. Introduction

Energy has become one of the hottest words in China. On the one hand, the demand for energy in China is rapidly increasing, since China has become the largest energy consumer and producer in the world (US Energy Information Administration, EIA; <http://www.eia.gov/>), whereas on the other, energy is closely associated with the environment. For example, coal and oil consumption in the country has resulted in very seriously bad air pollution impacts and environmental problems, which have been reported on in countless situations. Air pollution and smog in China have become one of the most contentious issue for the international media. Hundreds of millions of people in the world's most populous country are suffering the effects of this pollution, which is putting a lot of pressure on environmental and public health conditions in China. To mitigate these problems, China has to accelerate the adjustment of energy structure and to increase the share of clean sources in its energy mix. According to China's Action Plan for the Prevention and

16 Control of Air Pollution [1], China desires to reduce coal consumption to less
17 than 65% in terms of total energy consumption by 2017.

18 China has a very long coastline, possessing rich ocean resources, which
19 attach great importance to marine development and exploitation of renewable
20 energy. As important renewable types, ocean wind and wave energy not only
21 provide China with energy sources, but also resources with which to address
22 and relieve the challenge of energy demands with respect to the environment
23 , while implementing a sustained development strategy. As [2] mentioned,
24 renewables can also provide tools to address many pressing needs, including
25 improving energy security, reducing human health problems, and mitigating
26 against greenhouse gas emissions.

27 In recent times (decades), previous researchers have made great contribu-
28 tions toward the assessment of wind/wave energy potential for various seas
29 in many regions and countries, based on the analysis of wind/wave data col-
30 lected from buoys, remote sensing, numerical hindcasts, and combinations of
31 these sources. Included among these are the following studies: for the UK
32 [3, 4], Portugal [5–7], Sweden [8], Belgium [9], Spain [10–13], Ireland [14, 15],
33 Europe [16], the North Sea [9], the Baltic Sea [17, 18], the Red Sea [19], the
34 Caribbean [20], Australia [21, 22], Canada [23], Iran [24], India [25–29], Korea
35 [30], Singapore [31], Chile [32], the Hawaiian islands [33, 34], Southern New
36 England [35], California [36, 37], the Atlantic coast of the southeastern USA
37 [36, 38], the US Pacific Northwest [39], as well as for the global ocean (e.g.,
38 [40–44]). In addition, wave/wind energy resource assessment has also been
39 conducted for China [e.g., 45–54], and also including for Hongkong [55–58].

40 The region of interest in the present study is near the coast of Shenzhen,

41 located at the northern extreme of the South China Sea. Shenzhen shares a
42 border with Hong Kong to the south, is 160 km south of the provincial capital
43 of Guangzhou, and 70 km south of the industrial city of Dongguan. To the
44 west, the resort city of Zhuhai is a 60 km away, (see Fig. 1). Shenzhen was
45 the earliest of the five special economic zones in China, originally established
46 in 1979, and was given the right of provincial-level economic administration.
47 Since then, it has been one of the fastest growing cities in the world, and
48 eventually became one of the largest cities in the Pearl River Delta region
49 from the one-time small fishing village, and one of the economic powerhouses
50 of China, as well as of the largest manufacturing bases in the world. As a
51 result of this tremendous economic growth, the demand for energy is no
52 doubt correspondingly rapidly increasing. The first nuclear power plant in
53 China was built in the coast of Daya Bay (see Fig. 1), a coastal region of
54 Shenzhen. However, relative to the economic growth, the marine develop-
55 ment of Shenzhen has fallen far behind. It wasn't until 2014 that the city
56 local government put buoys in the surrounding waters to observe and moni-
57 tor the atmospheric and hydrodynamic climate of the region, and for use in
58 marine and meteorology environmental studies and forecasting, and so on.
59 The locations of the buoys have been shown to be reasonably representative
60 of the hydrodynamic climate of different areas in this region, in a limited ex-
61 penditure, and, from these, 6 buoy locations were selected (see section 2 for
62 details). This was a great progression and good start for marine observations
63 and monitoring for this region.

64 By means of data collected from six buoys located in the nearshore Shen-
65 zhen zone, this study aims to evaluate wind and wave climate for the region,

66 in terms of wind speed and direction, wave height, wave period and wave di-
67 rection. The potential of wind and wave energy as resources is assessed based
68 on buoy observations for the period 2014–2016. Location of the area of in-
69 terest and accumulated data at each of the six buoys, and also bathymetry
70 of the region are described in detail in section 2, where the methods for es-
71 timating wind and wave power are also presented. Wind and wave resource
72 variability in the region are investigated and discussed in section 3. Finally,
73 conclusions are presented in section 4.

74 **2. Data and methods**

75 *2.1. Study area and buoy data*

76 The region of wind and wave energy resource under investigation extends
77 from 22.0°N–23.0°N and 113.5°E–114.5°E (Fig. 1), and includes the entire
78 nearshore region of Shenzhen adjacent to Hong Kong. Six buoys, acquired
79 from Shenzhen Marine Monitoring Forecasting Center, are available in the
80 study region, and their locations and corresponding mean water depths are
81 listed in Table 1. Data from these buoys represent the wind and wave cli-
82 mate for different areas of the Shenzhen coastal region, mainly to monitor
83 atmospheric and hydrodynamic changes in this region and also to be used for
84 marine environmental investigating, forecasting, etc. The study area consists
85 of the waters extending from Shenzhen Bay in the northwest, southward and
86 eastward containing waters surrounding Hong Kong to Dapeng Bay, east of
87 Hong Kong and further east to include Daya Bay. The six buoys are located
88 very close to shore in very shallow water across the three bays: B1 is located
89 in the northwest end of Dapeng Bay in water depth of about 11 m; B2 is also

90 located in Dapeng Bay, close to the western side of Dapeng Peninsula; B3
91 is located in Aozaixia Bay in inner Daya Bay in water depth of only about
92 3 m; B5 is situated in southern Daya Bay (water depth: 12 m); B4 is located
93 in the relatively open area off the tip of Dapeng peninsula in water depth of
94 about 22 m; and B6 is located in inner Shenzhen Bay, in a relatively narrow
95 and closed area with water depth only 3 m.

96 The six buoys have been in operation since April 2014. Wave data were
97 provided hourly, consisting of wave parameters, including wave height, period
98 and direction. However, some wave data were not recorded over a span
99 of several days, and data gaps for each buoy can be inferred from Fig. 7.
100 Significant wave height (H_s), which is identical to the average of the highest
101 one-third of all wave heights recorded during each wave acquisition, is utilized
102 and analyzed for wave energy assessment in this study, while the measured
103 wave period acquired from buoy measurements refers to mean wave period,
104 T_m . However, only buoys B1–B4 and B6 provided records of wind data
105 (at 2.5 m above sea surface), including wind speed and direction at quarter-
106 hourly intervals, except for B4 (mainly half-hourly). Wind direction at B6
107 was also missed.

108 *2.2. Analytical methods and approach*

109 Wind power is defined as the power per unit section perpendicular to
110 wind flow, and is computed in this study by the following equation [52]:

$$W = \frac{1}{2}\rho_a V^3, \quad (1)$$

111 in which W is wind power in units of W m^{-2} , V is wind speed (unit: m s^{-1}),
112 and ρ_a is air density taken as 1.292 kg m^{-3} and corresponding to that close

113 to the sea surface in the region of interest in this study.

114 It was noticed that, for wave power calculations and assessments, the
115 widely used wave period is the so-called wave energy period, T_e , instead of
116 T_m . T_e can be defined as $T_e \equiv T_{-10} = \frac{m_{-1}}{m_0}$, in which m_n is the n^{th} moment
117 of spectral density, i.e., $m_n = \int_0^{2\pi} \int_0^\infty f^n S(f, \theta) df d\theta$, and here f is the wave
118 frequency, θ is the wave direction, and $S(f, \theta)$ is the 2D wave spectrum. In
119 general, the observed wave period measured by buoys for real sea states is
120 rarely specified by T_e , but is specified in terms of the mean wave period T_m , or
121 in terms of the peak period T_p . T_e is often estimated by means of its relation
122 to other observational wave periods, such as T_m and T_p , when the spectral
123 density is unknown [40]. Therefore, the relationship between T_e and T_p can
124 be estimated by the formula $T_e = \alpha T_p$, in which α depends on the shape of
125 the wave spectrum used to define the sea state. The relationship between
126 T_p and T_e used in this study is computed by a conservative approximation
127 that $T_e = 0.9T_p$, according to the study of [40]. This relationship has been
128 widely adopted in assessing the wave energy resource such as off the coast of
129 Canada [23], in the North Sea [9], and for the global ocean [40] as well as for
130 the offshore wave power in the East China Sea [54].

131 Based on the study of [8, 10–12, 28, 41, 54], the wave power, P , known
132 as wave energy flux as well, is calculated by the following expression

$$P = \frac{\rho_w g^2}{64\pi} H_s^2 T_e, \quad (2)$$

133 where ρ_w represents sea water density taken as 1025 kg m^{-3} , the average
134 sea water density in the study area. Since T_p was not provided in the buoy
135 records acquired in this study, T_m was used to estimate the wave power in the
136 region of interest. Following the study of [54, 59], the relationship between

137 T_m and T_p is adopted as $T_p = 1.2T_m$, and as a result, T_e investigated in the
138 present study is computed by means of T_m as $T_p = 0.9 \times 1.2T_m = 1.08T_m$.

139 **3. Results and Discussion**

140 *3.1. Wind climate and assessment of wind energy potential*

141 To assess the wind climate in the Shenzhen coastal region, the time series
142 of wind speeds based on the buoy measurement data (B1–B4 and B6) for the
143 period 2014–2016 is plotted by Fig. 2. It can be observed that wind speeds
144 in the study area were mostly less than 8 m s^{-1} for the 5 buoys except B4
145 buoy, where the wind speed was generally less than 10 m s^{-1} ; relatively high
146 wind speeds of greater than 15 m s^{-1} occurred occasionally. Based on Eq. 2,
147 Fig. 3 displays the calculated wind power for the 5 buoys. It shows that the
148 wind power for the 5 buoys (except B4) was mostly less than 300 W m^{-2} ,
149 while B4 shows relatively larger wind speeds, with values mostly smaller
150 than 500 W m^{-2} . Large wind power values of more than 3500 W m^{-2} can
151 occasionally be found in the observed time.

152 The fundamental characteristics of wind energy resources, in terms of
153 the annual mean wind speed with its standard deviation ($(V_{mean} \pm \text{std.dev.})$),
154 maximum wind speed (V_{max}), annual mean and maximum wind power (i.e.,
155 W_{mean} and W_{max}), is summarized in Table 1. In Dapeng bay, represented
156 by buoys B1 and B2, the annual mean wind speed during 2014–2016 was
157 3.1 m s^{-1} , and in Daya Bay, represented by B3, V_{mean} was 3.4 m s^{-1} ; simi-
158 larly, in Shenzhen bay, as B6 shows, V_{mean} was 3.6 m s^{-1} ; relatively stronger
159 wind speed was found at B4, with mean wind speed of 4.1 m s^{-1} . In ac-
160 cordance with the mean wind speed, the annual mean wind power, W_{mean} ,

161 at B1 and B2 was, respectively, 58 W m^{-2} and 37 W m^{-2} , and W_{mean} was
162 around 50 W m^{-2} in Daya bay and Shenzhen bay, highest W_{mean} among the
163 buoys was found at B4 with value of 94 W m^{-2} . V_{mean} averaged at the buoys
164 was about 3.5 m s^{-1} , leading to an average W_{mean} of around 58 W m^{-2} for
165 2014–2016.

166 For the period 2014–2016, maximum wind speed, V_{max} , at B1, B2, and
167 B4 was, respectively, 17.5 m s^{-1} , 17.6 m s^{-1} , 17.1 m s^{-1} , leading to wind power
168 of more than 3000 W m^{-2} , while V_{max} was relatively smaller at B3 and B6,
169 with values of 15.66 m s^{-1} and 15.7 m s^{-1} , respectively, giving a corresponding
170 W_{max} of over 2300 W m^{-2} .

171 It is noted that the study region is influenced by tropical cyclones (TCs;
172 normally called typhoons in China) relatively frequently, and they have been
173 reported many times. Therefore, the variance of maximum wind speeds can
174 be quite large for different time periods. Maximum wind speed depends
175 greatly on the extent and degree of the TC effects. For example, for the
176 period 2014–2016, 3 TCs passed through the study region that had much
177 influence it, see Fig. 4. The periods of these TCs are plotted in Fig. 2, and
178 it is observed that wind speeds in these time were relatively high. TCS are
179 normally classified into different categories. In China, in accordance with
180 the World Meteorological Organization’s recommendation, the classification
181 is divided into 6 categories by the classification of TCs standardization of
182 China (GB/T19201–2006 [60]), in terms of wind speed averaged over a pe-
183 riod of 10 minutes near the center of the TC. The six classifications are
184 as follows: Tropical Depression (TD; $10.8–17.1 \text{ m s}^{-1}$); Tropical Storm (TS;
185 $17.2–24.4 \text{ m s}^{-1}$); Severe Tropical Storm (STS; $24.5–32.6 \text{ m s}^{-1}$); Typhoon

186 (TY; $32.7\text{--}41.4\text{ m s}^{-1}$); Severe Typhoon (STY; $41.5\text{--}50.9\text{ m s}^{-1}$); and Super
187 Typhoon (SuperTY; $\geq 51.0\text{ m s}^{-1}$). Fig. 4 shows that TCs Nida (No. 1604)
188 and Haima (No. 1622) were in the classification of STY when they landed
189 (around Aug. 2 and Oct. 21 in 2016, respectively), and correspondingly, the
190 wind speeds could reach up to 15 m s^{-1} at B1, B2 and B4 locations, while
191 they were relatively small (about 10 m s^{-1}) at locations B3 and B6. Linfa
192 (No. 1510) was much weaker when it came to the Shenzhen region, and
193 its influence on wind speed was much less. The other 3 TCs displayed in
194 Fig. 4 were relatively far from the study region, but their influence is still
195 seen: wind speed at the 4 buoys were all relatively large with values reaching
196 15 m s^{-1} , in the influence of the Kalmaegi (No. 1415); the other two TCs
197 were also evident for the wind speeds in the study area.

198 The seasonal and monthly mean wind speed variations at the wind buoys
199 in the study area are presented by Fig. 5. For the present study, the four
200 boreal seasons are winter (December–February), spring (March–May), sum-
201 mer (June–August), and Autumn (September–November). The monthly
202 wind speeds over the period 2014–2016 varied from about $2\text{--}6\text{ m s}^{-1}$, with
203 different variability found at each of the buoys. Highest monthly mean wind
204 speeds occurred at station B4, with values of about 5.6 m s^{-1} in November
205 2015, followed by station B1 (5.2 m s^{-1} in December 2014). However, at lo-
206 cation B6 in Shenzhen Bay, the largest monthly wind speed was not found
207 in winter, but in June 2015 (4.3 m s^{-1}), followed by June 2016 (4.2 m s^{-1}),
208 while the smallest monthly value was reported in October 2016.

209 Corresponding to wind speeds, monthly mean wind powers at the 5 buoy
210 locations varied from 20 W m^{-2} to 200 W m^{-2} : relatively large wind powers

211 can be found in autumn and winter months at B1 and B4; while at B6 wind
212 powers in June and July were larger than those in winter months.

213 Fig. 5 also shows that the variation of monthly mean wind speeds and
214 powers within a year was largest at B1, followed by B4, and was smallest
215 at B3. Furthermore, no coincident seasonal variability was found in the
216 winds and the wind powers at any of the buoy locations for 2014–2016. Of
217 these, stations B1 and B4 show similar seasonality: winds and wind powers
218 were relatively large in autumn and winter, and were smaller in the spring
219 and summer months; however, B2 and B3 locations did not show evident
220 seasonality. Note that the data in some months for B2 was lacking, which
221 may influence the accuracy of its seasonality. On the contrary, B6 location
222 shows opposite seasonality when compared with B1 and B4 during the study
223 period: winds and wind powers were relatively large in spring and summer,
224 and were smaller in autumn and winter months.

225 Besides wind speed, wind direction is another important parameter in
226 wind energy assessment. For the data collected at the 6 buoys, only that at
227 buoys B1–B4 include wind direction data. Wind direction and wind speed
228 for different seasons at the 4 buoys is presented in terms of a wind rose figure,
229 Fig. 6. It can be seen that variability in wind direction is different for the
230 4 buoy locations. At location B1, in winter, easterly winds prevailed (about
231 31%), followed by winds directed from the ESE (about 28%), and occasionally
232 from the ENE and N (about 7%), whereas westerly winds are least frequent
233 (less than 5%); in spring, prevailing direction was from the II quadrant,
234 i.e., from E to S, with least occurrence also from the west; in autumn and
235 winter, winds were mostly southerly, followed by SSE and SSW directions,

236 respectively, and winds from land, i.e., from the IV and I quadrants, provided
237 the smallest contribution to the wind energy at B1. For B2, the prevailing
238 wind direction was easterly in all seasons (over 45%), followed by ENE, and
239 lowest occurrence occurred from SE to NW. At location B3 in Daya Bay, for
240 all seasons the largest contribution to wind energy resources was provided
241 by southerly winds, and SSE and SSW winds also provided considerable
242 contributions. At the B4 location, the prevailing wind direction varied for
243 all seasons, with almost all occurrence from each direction being less than
244 15%: in winter, most winds were from the the I quadrant followed by the
245 II quadrant; W (about 16%) prevailed in spring, followed by WSW (14%)
246 and WNW (13%); southerly winds prevailed in autumn, and winds from E
247 to W accounted for more than 75% of occurrence; in autumn, most winds
248 were from the III quadrant.

249 The occurrence of wind speed at the 4 buoy locations during 2014–2016
250 can also be observed from Fig. 6. For B1, the occurrence of wind with speed
251 less than 5 m s^{-1} was, respectively, about 85%, 88%, 90%, and 70% in the 4
252 seasons (winter, spring, summer and autumn); relatively large wind speeds
253 of over 8 m s^{-1} are mostly found in autumn (about 10%), followed by winter
254 (about 3%). For B2, around 86% of wind speed was less than 5 m s^{-1} in all
255 seasons except spring, when it was around 80%; the occurrence of wind speed
256 greater than 8 m s^{-1} was always less than 1% of the time in all seasons. At B3
257 wind speed was less than 5 m s^{-1} 80% of the time, while wind speed greater
258 than 8 m s^{-1} also occurred relatively rarely (less than 2% for all seasons).
259 Among the 4 buoys wind speed was greatest at B4, where wind speeds were
260 over 5 m s^{-1} in winter and autumn about 45% of the time, and 20% of the

261 time in summer and spring; the occurrence of wind speed over 8 ms^{-1} was,
262 respectively, about 10%, 3.6%, 3.8%, and 1.5% in winter, spring, summer
263 and autumn.

264 3.2. Wave climate and assessment of wave energy potential

265 In this section, wave state in terms of observed wave height and calculated
266 wave energy period is analyzed. Time series of significant wave height, H_s ,
267 and wave energy period, T_e , at the six buoys considered in this study are
268 presented in Fig. 7. It can be seen from this figure that H_s is relatively low
269 for most of the period 2014–2016. At the 6 buoy stations, H_s was less than
270 1 m, most of the time, and was even less than 0.5 m at buoy stations B2, B3,
271 and B6. It is not surprising that H_s is small in this region, since, first of all,
272 water depth is very small, and, secondly, the buoys are located in bays that
273 are somewhat semi-closed, all of which are not favorable for the development
274 of wind waves. Among these six buoys, H_s at B4 was relatively higher than
275 that at the others, which is to be expected since the water is deepest here
276 while being closer to the open South China Sea. Relatively higher values
277 exceeding 2 m are found only in some rare cases due to relatively strong winds
278 caused by tropical cyclones passing through the region, see discussion above.
279 For the period 2014–2016, no extreme waves (e.g., $H_s > 10 \text{ m}$) were observed,
280 even during periods of influence from tropical cyclones passing through.

281 T_e at the buoys is also presented in Fig. 7. In inner Dapeng Bay, repre-
282 sented by B1 and B2, T_e mostly varies between 3 s and 7 s, with occasional
283 values of more than 10 s. Similarly, at B5, in Daya bay, T_e was also mostly in
284 the range of 3–7 s. Relatively higher T_e was found at B4, with most values
285 between 4–7 s. In Aozaixia Bay (inner Daya Bay) represented by B3, T_e was

286 relatively small and mostly in the range 3–5 s, Similar values of T_e are found
287 in Shenzhen Bay represented by B6. Moreover, T_e values greater than 10 s
288 occasionally occurred at the 6 buoys, mostly due to the influence of tropical
289 cyclones.

290 Based on H_s and T_e , the wave power, P , was estimated at the 6 buoy
291 stations, Fig. 8. From comparison with time series of H_s shown in Fig. 7, the
292 temporal variations of P and H_s were basically coherent, at both hourly, daily
293 and monthly time scales. This can be explained from the relation of P and
294 H_s , since P is proportional to the square of H_s . For the period 2014–2016,
295 P was mostly confined to the range of 10^2 to 10^3 W m^{-1} at B1, B4 and B5,
296 while at B2, B3 and B6 wave power was considerably less, with values mostly
297 less than 100 W m^{-1} .

298 Statistics of annual wave climate at the six buoys were calculated and
299 are summarized in Table 1, in terms of annual mean significant wave height
300 and its standard deviation ($(H_s)_{mean} \pm \text{std.dev.}$), maximum significant wave
301 height ($(H_s)_{max}$), annual mean wave period ($(T_e)_{mean}$), and annual mean
302 and maximum wave power (i.e., P_{mean} and P_{max}). It was not surprising that
303 $(H_s)_{mean}$ averaged over the period 2014–2016 was very small, with values less
304 than 0.5 m for the buoys except B4, and $(H_s)_{mean}$ was only about 0.1 m at B3
305 and B6. B4 displays a relatively $(H_s)_{mean}$, but was still very small (0.6 m).
306 The largest $(H_s)_{max}$ was found at B4, with value of over 4.0 m, occurring on
307 September 16, 2014 when Typhoon Kalmaegi (No. 1415) passed through.
308 For Inner Dapeng Bay, represented by B1 and B2, $(H_s)_{max}$ was, respectively,
309 2.5 m and 2.4 m, and about 1.7 m at B5. Smallest $(H_s)_{max}$ was still found at
310 B3 and B6 (less than 1 m). $(T_e)_{mean}$ was relatively larger at B1, B2, B4 and

311 B5 (about 4.5 s), and smaller at B3 and B6 (3.5 s). The spatial distribution
312 of wave power was similar to that of H_s : annual mean and maximum wave
313 power, P_{mean} and P_{max} , were also largest at location B4 (1.25 kW m⁻¹ and
314 88.1 kW m⁻¹, respectively), followed by B5, B1, and B2 (respectively, 0.46,
315 0.39, 0.26 kW m⁻¹ for P_{mean}), while they were still smallest at B3 and B6
316 (0.03 kW m⁻¹ for P_{mean} , and 1.2 and 1.6 kW m⁻¹ for P_{max} , respectively).

317 Monthly and seasonal wave climate variability are of importance for wave
318 energy resource assessment. Monthly mean and seasonal characteristics of
319 H_s and T_e as well as P were thus investigated for the study region, based on
320 the buoy observations over the period 2014–2016.

321 Fig. 9 shows the variability in monthly values of H_s , T_e and P observed at
322 the 6 buoy locations, while also displaying spatial difference in these variables
323 between buoys. The monthly mean H_s for 2014–2016 can be briefly divided
324 into three groups: smallest monthly mean H_s was found at B6 and B3, with
325 values mostly less than 0.1 m; monthly mean values of H_s at B1, B2 and B5
326 were mostly in the range of 0.2 m–0.5 m; largest monthly values H_s occurred
327 at B5, which was between 0.5 m–0.8 m. Monthly mean values of T_e were also
328 smallest at B3 and B6 (mostly around 3.5 s), followed by T_e at B5 (between
329 4 s–5 s), while monthly T_e at B4, B2 and B1 were relatively large with values
330 ranging between 4.5 s–6.0 s. Correspondingly, monthly mean wave power,
331 P , for the period 2014–2016 at the 6 locations can also be also divided into
332 three groups by magnitude: largest at B4, with values ranging from about
333 1 kW m⁻¹ to 3.5 kW m⁻¹; monthly P were all less than 1 kW m⁻¹ at B1, B2
334 and B5; while very small values were recorded at B3 and B6, with magnitudes
335 of all less than 0.1 kW m⁻¹.

336 Seasonal values of H_s , T_e and P also displayed spatial variability be-
337 tween the six buoy locations (see Fig. 9). At locations B3 and B6, seasonal
338 variations in H_s , T_e and P were very small and limited in 0.1 m, 4 s and
339 0.1 kW m^{-1} , respectively. Seasonal differences in H_s , T_e and P were evident
340 at locations B1 and B5: seasonal values at B1 and B5 were relatively large
341 in autumn and winter, and smaller in spring and summer months. Relative
342 to B1 and B5, reversed seasonality was observed at B2, i.e., large values oc-
343 curred in summer months with smaller values observed in winter. Largest
344 seasonal values of H_s (around 0.6 m) were observed at B4, with relatively
345 small variability. However, larger values of T_e and P were recorded in sum-
346 mer and autumn months, with smaller values in winter and spring. From the
347 comparison between seasonal and monthly winds (Fig. 5) and waves (Fig. 9),
348 it is not surprising that the variability in the wind climate were not coherent
349 with those of the wave climate in the study region, since, in general, waves
350 in the coastal area might be not generated by local winds.

351 In addition to the numerical values of significant wave height and energy
352 period, their frequency of occurrence is also important for assessment of
353 wave energy resources. The combined scatter and energy diagrams, in terms
354 of H_s , T_e , and P , can provide convenient and comprehensive information
355 for conveying the characteristics of wave energy resources. Fig. 10 shows the
356 diagrams for the 6 sites, averaged at the same observational time (hourly) and
357 all based on the data 2014–2016. In the figure, the significant wave height
358 has been divided into intervals of one third of a meter in the range of 0–3 m,
359 and the energy period has been divided into intervals of 1 s ranging from 1 s
360 to 10 s. The colors on the diagrams show the proportion of incident energy

361 expected in one year, with numerical values given by the colour bar. The
362 black curves, n the values of 1 kW m^{-1} , 3 kW m^{-1} , and 5 kW m^{-1} , represent
363 isolines of wave power calculated from Eq. 2. The numerical values on the
364 diagrams in the figure represent the occurrence of a combination of H_s and
365 T_e within the corresponding range, in number of hours per year.

366 In Inner Dapeng bay, represented by buoys B1 and B2, Fig. 10 shows
367 that, for buoy B1, sea states in the range of 0.3–0.6 m for H_s and 5–6 s
368 for T_e occurred most frequently, providing the largest contribution to the
369 total annual wave energy (more than 30%), and the second largest contri-
370 bution (about 18%) was from sea states with H_s between 0.3–0.6 m and T_e
371 between 4–5 s, which also displayed high frequency of occurrence; at B1, the
372 frequency of occurrence of sea states with H_s between 0 m and 0.3 m and
373 T_e between 4 s and 6 s was also very high, while the contribution to the to-
374 tal wave energy was less than 20%, since their values are relatively small;
375 moreover, sea states of H_s between 0.3 m and 0.6 m and T_e between 6 s and
376 7 s at B1 provided a relatively high contribution of about 15% to the wave
377 energy, due to the relatively larger values in terms of H_s and T_e , even though
378 their frequency of occurrence was relatively low; for buoy B2, sea states with
379 highest frequency of occurrence were, respectively, in the range 0.0–0.3 m
380 for H_s and 4–6 s for T_e , and together they contributed more than 30% of
381 total wave energy resources, while sea states of H_s between 0.3–0.6 m and
382 T_e between 5–6 s provided a significant contribution (more than 20%) to the
383 wave energy resource, followed by the contribution from sea states of H_s and
384 T_e , respectively, in the range of 0.3–0.6 m and 6–7 s.

385 Concerning sea states, Fig. 10 clearly shows that for B3, located in Aoza-

386 ixia Bay, within Daya bay, almost all sea states were below 0.3 m and in
387 the range 6–7 s, in terms of H_s and T_e , respectively, and contributing more
388 than 60% of total wave energy resources there, with the second most signifi-
389 cant contribution coming from sea states of H_s less than 0.3 m and T_e 4 s to
390 5 s. For the other buoy station in Daya Bay, B5, sea states with the high-
391 est frequency of occurrence were in the range 0.0–0.3 m and 4–5 s for H_s
392 and T_e , respectively, providing the largest contribution to the total annual
393 wave energy (more than 43%); with the second largest contribution (about
394 30%) coming from sea states with H_s and T_e between 0–0.3 m and 5–6 s,
395 respectively; the frequency of occurrence of sea states with H_s below 0.3 m
396 were also significantly high, but their contribution to the total annual energy
397 resources was relatively small.

398 For buoy B4, located off the coast of Dapeng peninsula and in the deepest
399 location of the 6 buoys, sea states in the range of 0.3–0.9 m for H_s and 4–6 s
400 for T_e provided the largest contribution to the total annual wave energy (all
401 together more than 70%), while sea states with larger H_s , between 0.9–1.2 m,
402 and T_e between 5–6 s contributed about 8% of total wave energy resources.
403 For B6, located in the narrow Shenzhen Bay, sea states in terms of H_s and
404 T_e , and their contributions to total wave energy, were similar to those at
405 location B3, where water depth is also very shallow as well.

406 Overall, for all buoys, most sea states in terms of H_s were below 0.6 m.,
407 Concerning T_e , most sea state values were between 4–6 s for B1–B2, and
408 B4–B5, while values of between 3–4 s were found for B3 and B6. A basic
409 knowledge of significant wave height values informs that values below 0.6 m
410 in the ocean are quite small. It is not surprising that H_s is small in the

411 study region, since water depths are correspondingly low and the region is
412 relatively closed off from open seas.

413 Wave direction plays an important role in wave energy assessment. Fig. 11
414 shows seasonal distributions of incoming wave direction for the 6 buoys in
415 the study region. It is apparent from this figure that there was no obvious
416 seasonal change in wave direction for the 6 buoys. Wave directions at these
417 buoys locations were not in accordance with the corresponding wind direc-
418 tions (see Fig. 6), but they mainly reflected the wave propagating directions
419 of propagating away from generation sources in the open region towards the
420 coast, so that none at all was from the IV quadrant due to the coastline
421 orientations at the buoys. Moreover, in all directions wave power was mostly
422 less than 1 kW m^{-1} .

423 In Dapeng bay, most waves came from the II quadrant: for B1, the pre-
424 vailing wave direction was from the SE, with a very minor contribution from
425 the SSE; for B2, southerly waves prevail in all seasons except in Winter, fol-
426 lowed by SSW, whereas SSW waves a little more occurred in winter, with a
427 little lower occurrence (about 31%) from the south. For Daya bay, at B3,
428 most of the wave energy was provided by waves from the I quadrant, and
429 the prevailing wave direction was NE, followed by ENE and NNE, which did
430 not match the prevailing wind direction (see Fig. 6). This indicates that
431 the waves at B3 were mostly not generated by local winds, but mostly came
432 from the open region where the waves propagated to the coast. As for the
433 other buoy in Daya bay, B5, most of the wave energy was contributed by
434 easterly waves: ESE waves prevailed in winter and autumn, followed by N,
435 whereas northerly waves occurred more in Spring and summer, followed by

436 ESE; a minor contribution (less than 5%) was due to waves from the ENE.
437 At B4, Fig. 6 reveals that most waves came from the II quadrant, which
438 did not match the prevailing wind directions, indicating that the waves were
439 not generated by local winds, but from waves propagating away from gen-
440 eration sources in the open region. For B6 located in Shenzhen Bay, most
441 of the waves (more than 50% on average for the all seasons) came from III,
442 as expected, with southwesterly and WSW directions prevailing. However,
443 it is noted that occurrence from other directions was rare, especially from
444 the opposite direction, i.e., NE and ENE, which might be due to the fact
445 that this is a relatively narrow area, and where the influence of reflected and
446 refracted waves might be of more significance.

447 Previous studies have shown that waves transport energy supplied to
448 them over vast distances, and dissipative effects may play only a smaller role
449 in deep water, as opposed to the surf zone; nearshore waves are nonlinearly
450 related to the strength, fetch, and duration of the wind [62]. Therefore, the
451 local wave climate can be frequently affected by strong incident waves or
452 wind fetch both inside and outside the study region.

453 Last but not least, we provide a brief discussion concerning the relation-
454 ship between the wind energy and the wave climate for the study area. Fig. 12
455 displays a preliminary correlation between the wind speed/energy and the
456 wave climate based on the local buoy measurements. Results from all buoys
457 other than B5 (not recorded) are displayed. The upper panels of Fig. 12 show
458 the relationship between anomalies of monthly averaged data (monthly val-
459 ues minus monthly climatology) of wind speed and significant wave height for
460 the period 2014–2016. For this long-timescale (low frequency) comparison,

461 the threshold correlation coefficient at the 95% and 99% significance levels
462 is about 0.35 and 0.45, respectively (the sample of the time series of the
463 monthly anomalies is about 30). It can be seen from this figure that, except
464 at B3 buoy location, all other locations display a relatively small correla-
465 tion between wind strength and wave conditions. Moreover, we attempted
466 to calculate the delay/forward correlations, but they are still insignificant
467 (not shown). The bottom panel in Fig. 12 describes correlations between
468 daily anomalies (daily values minus monthly climatology) of wind speed and
469 H_s for the period 2014–2016. The coefficients were all statistically signifi-
470 cant (sample numbers for the time series are all greater than 550, and the
471 threshold correlation coefficient at the 95% and 99% significance levels is less
472 than 0.11). At Dapeng Bay, represented by buoys B1 and B2, correlations
473 were over 0.3 for the period 2014–2016. At B3, located in Daya Bay, the
474 correlation was very high, 0.77. A relatively high correlation is also found at
475 station B4 (0.60). For Shenzhen Bay (B6), the correlation coefficient is about
476 0.39, similar to values for Dapeng Bay. Therefore, at this daily timescale, the
477 local wind energy significantly influences the wave climate in the study area.
478 Thus, care must be taken before we can conclude whether the wave climate in
479 the study region might be more affected by the local wind at daily timescale
480 rather than for long-time statistics when non-local wave signals from outside
481 the study region get more involved.

482 **4. Summary and Conclusions**

483 In this study, wind and wave climates for the Shenzhen coastal region are
484 evaluated by means of buoy observational data. Buoys were first placed in

485 the region by the city local government in 2014 to observe and monitor the
486 atmospheric and hydrodynamic climate of the region. Six buoys are located
487 in different areas of the study region, including Dapeng Bay, Daya Bay,
488 Shenzhen Bay, and the area off the tip of the Dapeng peninsula. The waters
489 in these areas are very shallow, ranging in depth from about 3 m–22 m.

490 In terms of wind speed and direction at the buoys (2.5 m above the sea
491 surface), wind climate and potential wind energy resources were assessed in
492 detail for the period 2014–2016. It was found that the annual mean wind
493 speed at the buoy locations for the period 2014–2016 varied from about
494 3.1 m s^{-1} to 4.1 m s^{-1} , with maximum wind speeds of more than 17 m s^{-1} oc-
495 ccurring as a result of tropical cyclones. These winds resulted in annual mean
496 wind powers of about $37\text{--}94 \text{ W m}^{-2}$. Among the buoys, largest averaged
497 wind speed and power were found at B4, located in the relatively open area
498 off the southern coast of Dapeng peninsula. On average, more than 80% of
499 wind speeds were less than 5 m s^{-1} in the study region. However, the wind
500 speed was relatively large at location B4, where about 45% of wind speeds
501 were over 5 m s^{-1} in winter and autumn, and 20% in summer and spring.

502 Seasonal variability in wind speed and power fluctuated at the different
503 buoy locations over the 2014–2016 period. At B1 and B4, seasonal variability
504 was relatively large in autumn and winter, and smaller in spring and summer
505 months. However, reversed seasonality occurred at location B6, where wind
506 and wind power were relatively large in spring and summer, and were smaller
507 in autumn and winter. Seasonal variations were relatively small at B2 and
508 B3 locations.

509 Seasonal and spatial wind direction variability differed between buoys

510 B1–B4 (no wind direction data at B5 and B6). At B1, located in the north-
511 west end of Dapeng Bay, the prevailing wind direction in winter, spring, sum-
512 mer and autumn was, respectively, easterly, easterly to southerly, southerly,
513 and southerly. The prevailing wind direction was from the east in all seasons
514 at location B2. At B3, located in Daya Bay, the largest contribution to wind
515 energy resources was provided by the southerly winds, in all seasons, with
516 SSE and SSW winds also providing considerable contributions. The prevail-
517 ing wind direction at B4 varied seasonally, with occurrence of less than 15%
518 from any particular direction: in winter, most winds were from the the I
519 quadrant, followed by the II quadrant; westerly winds prevailed in spring,
520 with southerly winds prevailing in autumn.

521 Wave climate and potential wave energy resources in terms of wave height,
522 wave energy period, wave direction, and wave power were also evaluated for
523 the period 2014–2016. The data showed that at the 6 buoy locations, H_s was
524 mostly less than 1 m, and even less than 0.5 m at B2, B3, and B6 locations.
525 As a result, wave power, P , was mostly limited to the range 10^2 to 10^3 W m^{-1}
526 at B1, B4 and B5, and mostly less than 100 W m^{-1} at the other locations.
527 This may be due to the facts that, first, water depth is very shallow, and,
528 secondly, the buoys are located in bays where the sea is somewhat semi-
529 enclosed, all of which are not favorable for the development of wind waves.
530 T_e was mostly in the range of 3–7 s in the study region, with values of more
531 than 10 s occasionally occurring at all 6 buoys, mostly during periods of
532 tropical cyclones.

533 It was not surprising that annual mean significant wave height, $(H_s)_{mean}$,
534 for the period 2014–2016 was relatively small, with values of less than 1.0 m

535 for the study region, and largest values of (H_s) found at B4 of over 4.0 m.
536 In addition, most sea states in terms of H_s were less than 0.6 m, with T_e
537 between 4–6 s for B1–B2, and B4–B5, and 3–4 s for B3 and B6. The
538 annual mean wave energy period, $(T_e)_{mean}$, was relatively large at B1, B2,
539 B4 and B5 (about 4.5 s), and smaller at B3 and B6 (3.5 s). Correspondingly,
540 the annual mean wave power was largest at B4 (1.25 kW m^{-1}), and between
541 $0.26\text{--}0.46 \text{ kW m}^{-1}$ at B1, B2, and B5, and smallest at B3 and B6, with values
542 of only 0.03 kW m^{-1} . Therefore, we can conclude that the potential of the
543 wave energy resource at the buoy locations are very small.

544 **Acknowledgements**

545 X. Chen was funded by the National Natural Science Foundation of China
546 (NSFC) grant 41506042. Y. Zhang was funded by the NSFC grant 51609043
547 and by Key Laboratory of Coastal Disaster and Defense, Ministry of Educa-
548 tion, China, under the award 2016001.

549 **References**

- 550 [1] China's Action Plan on Prevention and Control of Air Pollution. the
551 State Council of the People's Republic of China; 2013.
- 552 [2] REN21. RENEWABLES 2015: Global Status Report (the Renewable
553 Energy Policy Network for the 21st Century). REN21; 2015.
- 554 [3] Atlas of UK Marine Renewable Energy Resources. Technical Report,
555 Report No.1432; 2008.
- 556 [4] Higgins P, Foley A. The evolution of offshore wind power in the United
557 Kingdom. *Renewable and Sustainable Energy Reviews* 2014;37:599–612.
- 558 [5] Mollison D, Pontes MT. Assessing the Portuguese wave-power resource.
559 *Energy* 1992;17(3):255–68.
- 560 [6] Rusu E, Guedes Soares C. Numerical modelling to estimate the spatial
561 distribution of the wave energy in the Portuguese nearshore. *Renewable*
562 *Energy* 2009;34(6):1501–16.
- 563 [7] Mota P, Pinto JP. Wave energy potential along the western Portuguese
564 coast. *Renewable Energy* 2014;71:8–17.
- 565 [8] Waters R, Engström J, Isberg J, Leijon M. Wave climate off the Swedish
566 west coast. *Renewable Energy* 2009;34(6):1600–6.
- 567 [9] Beels C, De Rouck J, Verhaeghe H, Geeraerts J, Dumon G. Wave energy
568 on the Belgian continental shelf. In: *Oceans 2007-Europe*. IEEE; 2007.
569 p. 1–6.

- 570 [10] Iglesias G, López M, Carballo R, Castro A, Fraguera JA, Frigaard
571 P. Wave energy potential in Galicia (NW Spain). *Renewable Energy*
572 2009;34(11):2323–33.
- 573 [11] Iglesias G, Carballo R. Wave energy resource in the Estaca de Bares
574 area (Spain). *Renewable Energy* 2010;35(7):1574–84.
- 575 [12] Iglesias G, Carballo R. Offshore and inshore wave energy assessment:
576 Asturias (N Spain). *Energy* 2010;35(5):1964–72.
- 577 [13] López-Ruiz A, Bergillos RJ, Ortega-Sánchez M. The importance of wave
578 climate forecasting on the decision-making process for nearshore wave
579 energy exploitation. *Applied Energy* 2016;182:191–203.
- 580 [14] Foley AM, Kerlin C, Leahy PG. Offshore wind resource estimation using
581 wave buoy data; 2012. p. 1114–19.
- 582 [15] Gallagher S, Tiron R, Whelan E, Gleeson E, Dias F, McGrath R. The
583 nearshore wind and wave energy potential of Ireland: A high reso-
584 lution assessment of availability and accessibility. *Renewable Energy*
585 2016;88:494–516.
- 586 [16] Clément A, McCullen P, Falcão A, Fiorentino A, Gardner F, Hammar-
587 lund K, et al. Wave energy in Europe: current status and perspectives.
588 *Renewable and Sustainable Energy Reviews* 2002;6(5):405–31.
- 589 [17] Henfridsson U, Neimane V, Strand K, Kapper R, Bernhoff H, Danielsson
590 O, et al. Wave energy potential in the Baltic Sea and the Danish part
591 of the North Sea, with reflections on the Skagerrak. *Renewable Energy*
592 2007;32(12):2069–84.

- 593 [18] Akpınar A, Komurcu MI. Assessment of wave energy resource of the
594 Black sea based on 15-year numerical hindcast data. *Applied Energy*
595 2013;101:502–12.
- 596 [19] Langodan S, Viswanadhapalli Y, Dasari HP, and Ibrahim Hoteit OK. A
597 high-resolution assessment of wind and wave energy potentials in the
598 Red Sea. *Applied Energy* 2016;181:244–55.
- 599 [20] Appendini CM, Urbano-Latorre CP, Figueroa B, Dagua-Paz CJ, Torres-
600 Freyermuth A, Salles P. Wave energy potential assessment in the
601 Caribbean Low Level Jet using wave hindcast information. *Applied*
602 *Energy* 2015;137:375–84.
- 603 [21] Hughes MG, Heap AD. National-scale wave energy resource assessment
604 for Australia. *Renewable Energy* 2010;35(8):1783–91.
- 605 [22] Morim J, Cartwright N, Etemad-Shahidi A, Strauss D, Hemer M. Wave
606 energy resource assessment along the Southeast coast of Australia on
607 the basis of a 31-year hindcast. *Applied Energy* 2016;184:276–97.
- 608 [23] Cornett AM. Inventory of Canada’s offshore wave energy resources.
609 In: 25th International Conference on Offshore Mechanics and Arctic
610 Engineering. American Society of Mechanical Engineers; 2006. p. 353–
611 62.
- 612 [24] Abbaspour M, Rahimi R. Iran atlas of offshore renewable energies.
613 *Renewable Energy* 2011;36:388–398.
- 614 [25] Baba M. Wave power potential off the south-west Indian coast. *Energy*
615 1987;12(6):501–7.

- 616 [26] Sivaramakrishnan TR. Wave power over the Indian seas during the
617 southwest monsoon season. *Energy* 1992;17(6):625–7.
- 618 [27] Kumar VS, Dubhashi KK, Nair TMB, Singh J. Wave power potential at
619 few shallow water locations around Indian coast. *Current Science India*
620 2013;104(9):1219–24.
- 621 [28] Kumar VS, Anoop TR. Wave energy resource assessment for the Indian
622 shelf seas. *Renewable Energy* 2015;76:212–219.
- 623 [29] Gadad S, Deka PC. Offshore wind power resource assessment using
624 Oceansat-2 scatterometer data at a regional scale. *Applied Energy*
625 2016;176:157–70.
- 626 [30] Oh KY, Kim JY, Lee JK, Ryu MS, Lee JS. An assessment of wind energy
627 potential at the demonstration offshore wind farm in Korea. *Energy*
628 2012;46:555–63.
- 629 [31] Karthikeya BR, Negi PS, Srikanth N. Wind resource assessment for
630 urban renewable energy application in Singapore. *Renewable Energy*
631 2016;87:403–14.
- 632 [32] Watts D, Osés N, Pérez R. Assessment of wind energy potential in Chile:
633 A project-based regional wind supply function approach. *Renewable*
634 *Energy* 2016;96:738–55.
- 635 [33] Hagerman G. Wave Energy resource and economic Assessment for the
636 State of Hawaii. Prepared by SEASUN Power Systems for the Depart-
637 ment of Business, Economic Development, and Tourism, Final Report;
638 1992.

- 639 [34] Stopa JE, Filipot JF, Li N, Cheung KF, Chen YL, Vega L. Wave
640 energy resources along the Hawaiian Island chain. *Renewable Energy*
641 2013;55:305–321.
- 642 [35] Hagerman G. Southern New England wave energy resource potential.
643 *Proc. Building Energy 2001, Boston, USA; 2001.*
- 644 [36] Beyene A, Wilson JH. Comparison of wave energy flux for northern,
645 central, and southern coast of California based on long-term statistical
646 wave data. *Energy* 2006;31(12):1856–69.
- 647 [37] Wilson JH, Beyene A. California wave energy resource evaluation. *Jour-*
648 *nal of Coastal Research* 2007;p. 679–90.
- 649 [38] Defne Z, Haas KA, Fritz HM. Wave power potential along the Atlantic
650 coast of the southeastern USA. *Renewable Energy* 2009;34(10):2197–
651 205.
- 652 [39] Lenee-Bluhm P, Paasch R, Özkan-Haller H. Characterizing the wave
653 energy resource of the US Pacific Northwest. *Renewable Energy*
654 2011;36(8):2106–19.
- 655 [40] Cornett AM, et al. A global wave energy resource assessment. In: *Pro-*
656 *ceedings of the Eighteenth International Offshore and Polar Engineering*
657 *Conference, Vancouver, Canada; 2008. p. 1–9.*
- 658 [41] Mork G, Barstow S, Kabuth A, Pontes MT. Assessing the global wave
659 energy potential. In: *ASME 2010 29th International Conference on*
660 *Ocean, Offshore and Arctic Engineering. American Society of Mechan-*
661 *ical Engineers; 2010. p. 447–54.*

- 662 [42] Gunn K, Stock-Williams C. Quantifying the global wave power resource.
663 Renewable Energy 2012;44:296–304.
- 664 [43] Arinaga RA, Cheung KF. Atlas of global wave energy from 10 years of
665 reanalysis and hindcast data. Renewable Energy 2012;39:49–64.
- 666 [44] Reguero BG, Losada IJ, Méndez FJ. A global wave power resource
667 and its seasonal, interannual and long-term variability. Applied Energy
668 2015;148:366–80.
- 669 [45] Zhou W, Yang H, Fang Z. Wind power potential and characteristic
670 analysis of the Pearl River Delta region, China. Renewable Energy
671 ;31(6).
- 672 [46] Li J, Gao H, Shi P, Shi J, Ma L, Qin H. China wind power report 2007;
673 2007.
- 674 [47] Zhang D, Li W, Lin Y. Wave energy in China: Current status and
675 perspectives. Renewable energy 2009;34(10):2089–92.
- 676 [48] Xia C, Song Z. Wind energy in China: current scenario and future
677 perspectives. Renewable and Sustainable Energy Reviews 2009;13:1966–
678 74.
- 679 [49] Han J, Arthur PJM, Lu Y, Zhang L. Onshore wind power develop-
680 ment in China: challenges behind a successful story. Energy Policy
681 2009;37:2941–51.
- 682 [50] Rajgor G. China gets serious on offshore wind. Renewable Energy Focus
683 2010;September/October.

- 684 [51] Wang S, Yuan P, Li D, Jiao Y. An overview of ocean renewable energy in
685 China. *Renewable and Sustainable Energy Reviews* 2011;15(1):91–111.
- 686 [52] Zheng C, Zhuang H, Li X, Li X. Wind energy and wave energy resources
687 assessment in the East China Sea and South China Sea. *Science China
688 Technological Sciences* 2012;55(1):163–73.
- 689 [53] Jiang D, Zhuang D, Huang Y, Wang J, Fu J. Evaluating the spatio-
690 temporal variation of China’s offshore wind resources based on remotely
691 sensed wind field data. *Renewable and Sustainable Energy Reviews*
692 2013;24:142–148.
- 693 [54] Wu S, Liu C, Chen X. Offshore wave energy resource assessment in the
694 East China Sea. *Renewable Energy* 2015;76:628–36.
- 695 [55] Li G. Feasibility of large scale offshore wind power for Hong Kong a
696 preliminary study. *Renewable Energy* 2000;21(3):387–402.
- 697 [56] Lu L, Yang H, Burnett J. Investigation on wind power potential on
698 Hong Kong islands a
699 an analysis of wind power and wind turbine characteristics. *Renewable Energy* 2002;27(1):1–12.
- 700 [57] Gao X, Yang H, Lu L. Study on offshore wind power potential and wind
701 farm optimization in Hong Kong. *Energy* 2014;130:519–31.
- 702 [58] Shu ZR, Li QS, Chan PW. Investigation of offshore wind energy po-
703 tential in Hong Kong based on Weibull distribution function. *Applied
704 Energy* 2015;156:362–73.

- 705 [59] Roger B. Wave energy forecasting accuracy as a function of forecast time
706 horizon; 2009.
- 707 [60] Committee CSA. Classification of tropical cyclones (GB/T19201-2006);
708 2006.
- 709 [61] Ying M, Zhang W, Yu H, Lu X, Feng J, Fan Y, et al. An Overview
710 of the China Meteorological Administration Tropical Cyclone Database.
711 Journal of Atmospheric and Oceanic Technology 2013;(2013).
- 712 [62] Zhang Y, Kennedy AB, Tomiczek T, Donahue AS, Westerink JJ. Val-
713 idation of Boussinesq-Green-Naghdi Modelling for Surf Zone Hydrody-
714 namics. Ocean Engineering 2016;111:299–309.

Table 1: List of measurement buoys in the Shenzhen coastal region with water depth and some fundamental mean wind and wave characteristics. The collected buoy data covered from April 2014 to the end of 2016, with data gap that can be seen in Fig. 2. Main wind and wave characteristics were statistically calculated, including wind speed, V (m s^{-1}); wind power, W (W m^{-2}); significant wave height, H_s (m); wave energy period, T_e (s); wave power, P (kW m^{-1}).

Buoy	Depth (m)	V_{mean} \pm std.dev.	V_{max}	W_{mean}	W_{max}	$(H_s)_{mean}$ \pm std.dev.	$(H_s)_{max}$	$(T_e)_{mean}$	P_{mean}	P_{max}
B1	11	3.1 ± 2.3	17.5	58	3282	0.34 ± 0.18	2.5	4.7	0.39	22.5
B2	11	3.1 ± 1.7	17.6	37	3339	0.25 ± 0.17	2.4	4.7	0.26	28.0
B3	5	3.4 ± 2.0	15.6	52	2325	0.11 ± 0.05	0.8	3.5	0.03	1.2
B4	22	4.1 ± 2.5	17.1	94	3063	0.62 ± 0.30	4.3	4.5	1.25	88.1
B5	12	/	/	/	/	0.38 ± 0.23	1.7	4.3	0.46	8.7
B6	3	3.6 ± 1.8	15.7	51	2347	0.13 ± 0.05	0.9	3.5	0.03	1.6

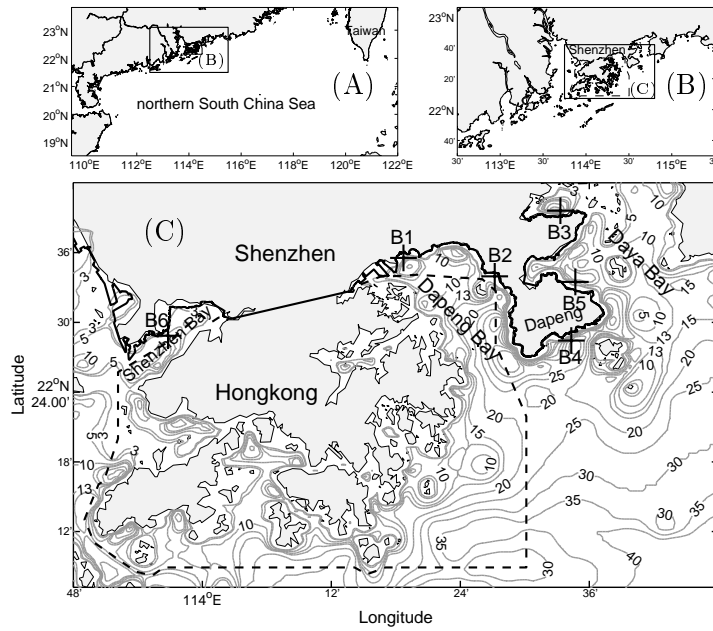


Figure 1: (C): Bathymetry contours (m) for the study area together with locations of the six wind and wave measurement buoys (B1-B6) in the coastal Shenzhen region (bottom/main panel). The study area is situated in the northern South China Sea (top panels). The broken line represents the boundary of Hong Kong waters.

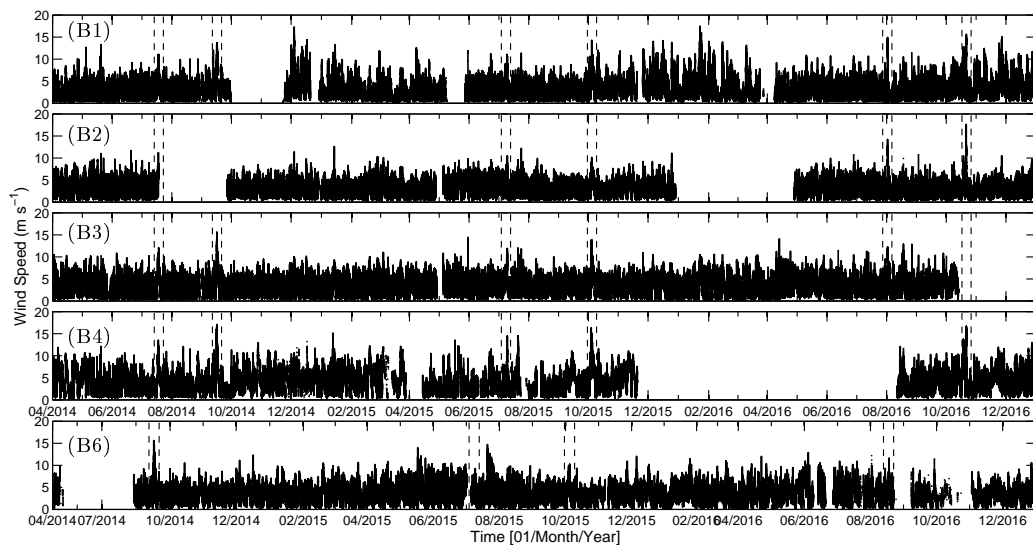


Figure 2: Time series of wind speed (m s^{-1}) at the buoy locations (B1–B4 and B6) shown in Fig. 1 for the period 2014–2016. Dashed lines show the time periods of the tropical cyclones (see Fig. 4) passing through the study region. Wind data were missed at B5 buoy.

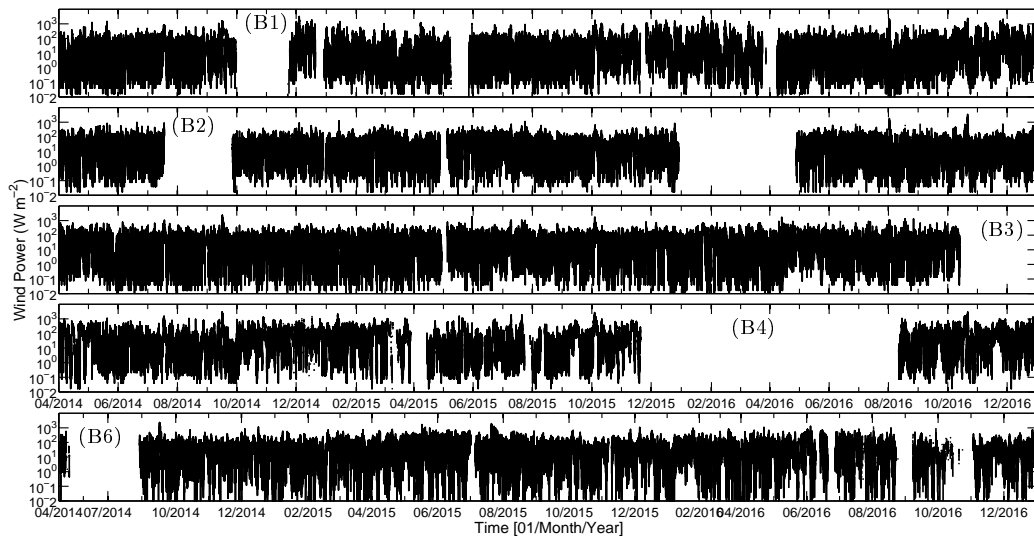


Figure 3: Time series of wind power (W m^{-2}) at locations B1–B4 and B6 shown in Fig. 1 for the period 2014–2016.

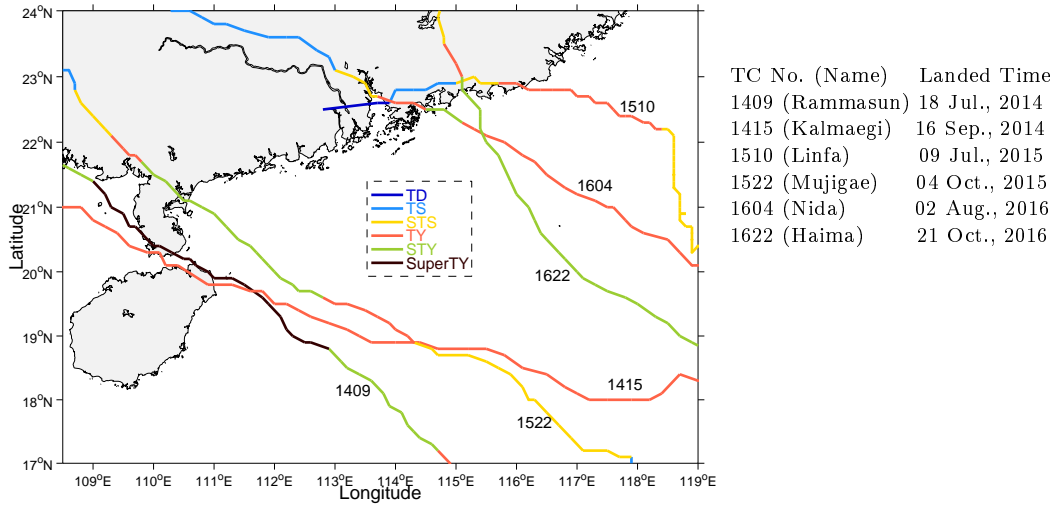


Figure 4: Left: Paths of tropical cyclones (TCs) passing through the northern South China Sea for the period 2014–2016. Right: The TC No. (Name) and landed time. Data source: http://tcdata.typhoon.gov.cn/zj1jsjj_sm.html [61]. The classifications of the TCs in China are as follows: Tropical Depression (TD; $10.8\text{--}17.1\text{ m s}^{-1}$); Tropical Storm (TS; $17.2\text{--}24.4\text{ m s}^{-1}$); Severe Tropical Storm (STS; $24.5\text{--}32.6\text{ m s}^{-1}$); TYphoon (TY; $32.7\text{--}41.4\text{ m s}^{-1}$); Severe TYphoon (STY; $41.5\text{--}50.9\text{ m s}^{-1}$); and Super TYphoon (SuperTY; $\geq 51.0\text{ m s}^{-1}$)

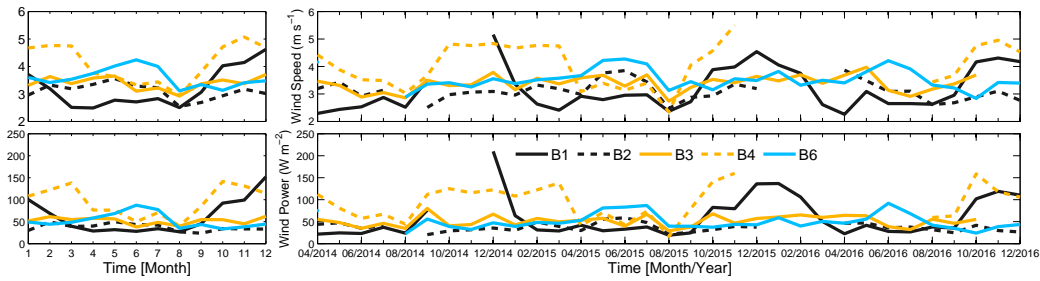


Figure 5: Seasonal (left) and monthly (right) mean wind speed (m s^{-1}) and wind power (W m^{-2}) for the buoys B1–B4 and B6 shown in Fig. 1.

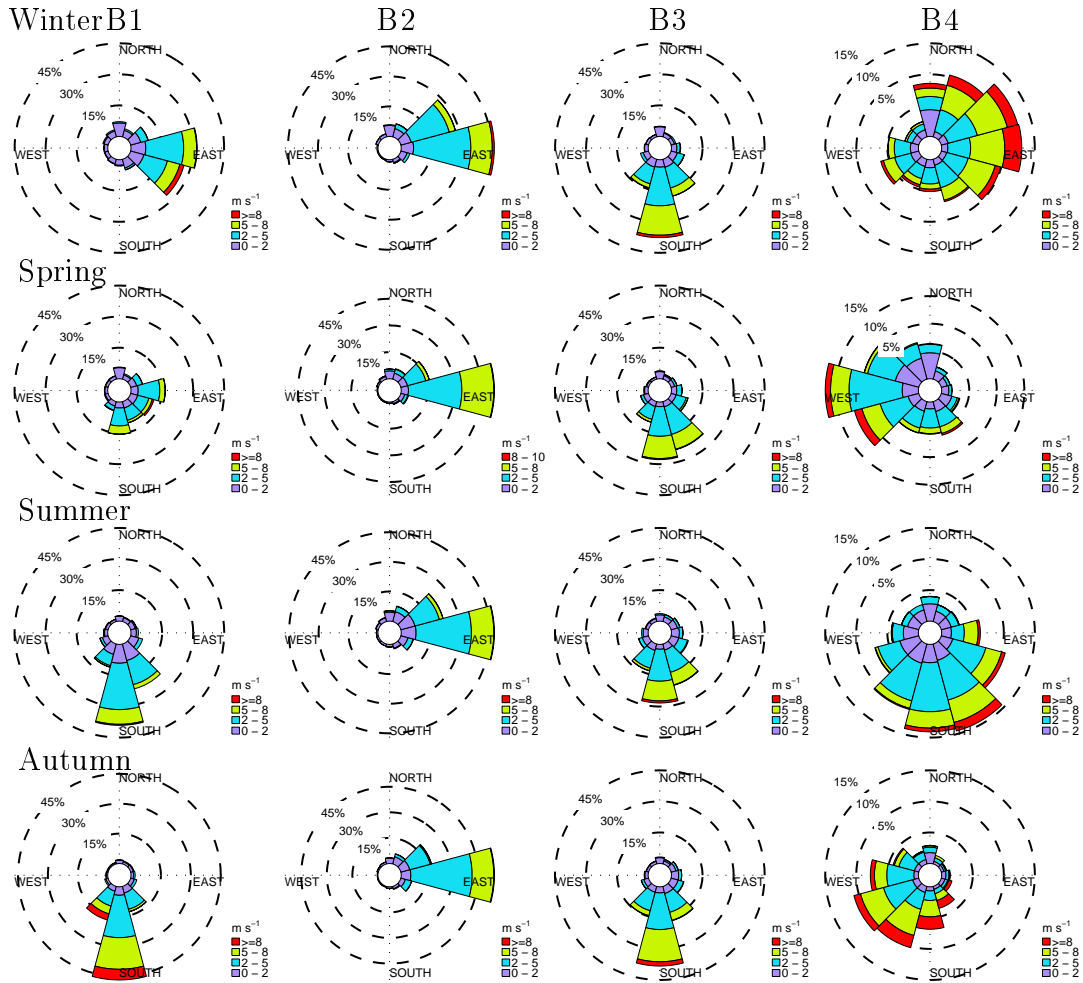


Figure 6: Seasonal wind speed and direction roses based on the measurement from buoys B1–B4 for the period 2014–2016. Wind direction data were missed at B5 and B6 locations.

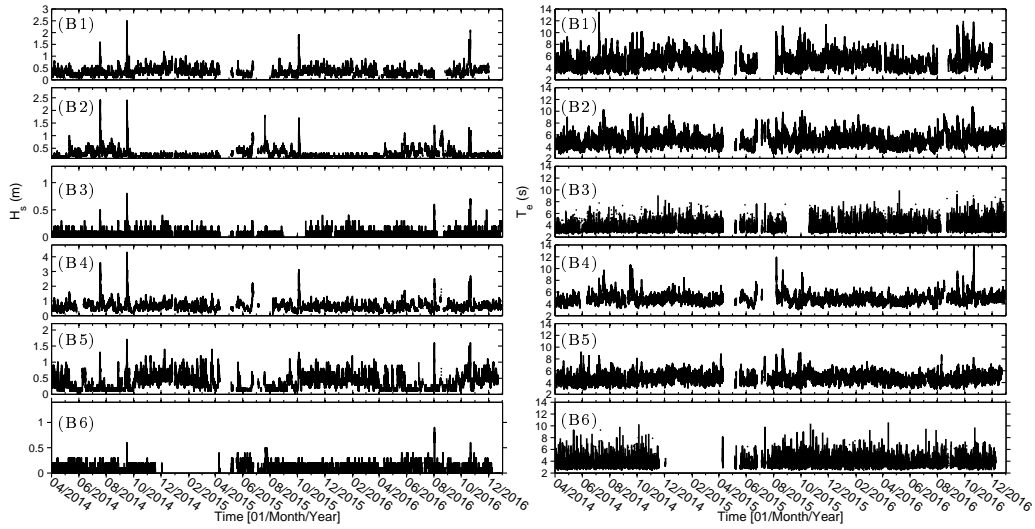


Figure 7: Time series of significant wave heights (H_s in m) and wave energy periods (T_e in s) at the six buoy locations (B1–B6) for the period 2014–2016.

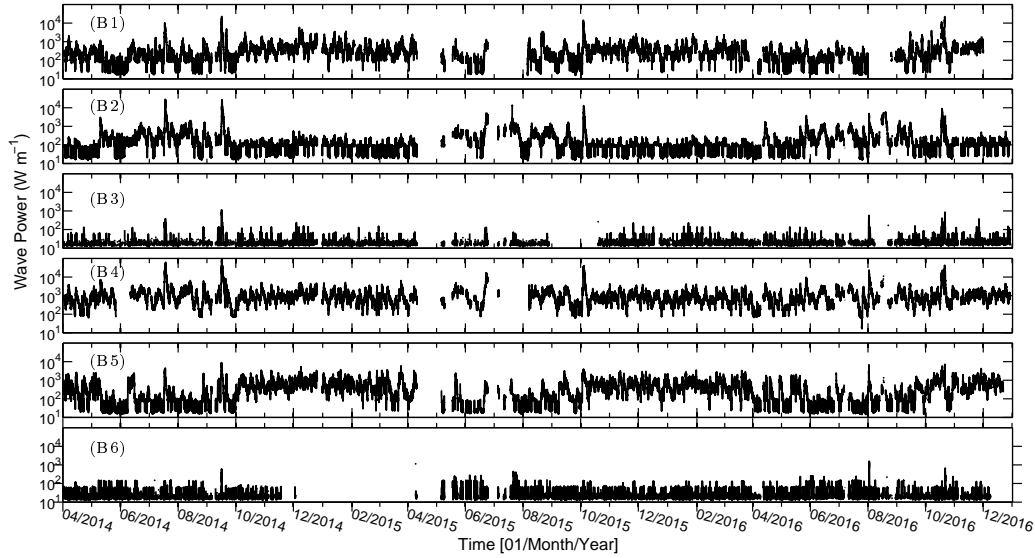


Figure 8: Time series of wave power (W m^{-1}), P , at buoy locations of B1–B6 shown in Fig. 1 for the period 2014–2016.

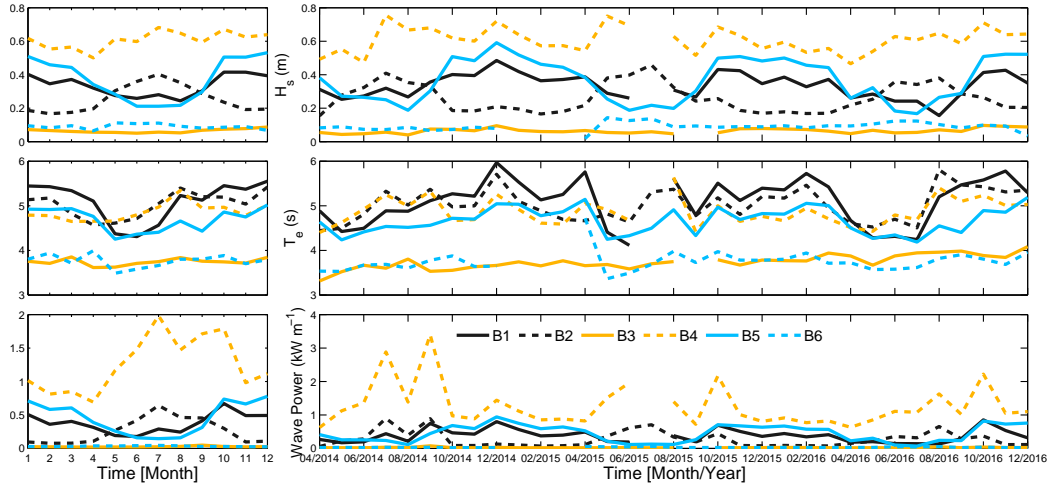


Figure 9: Seasonal (left) and monthly (right) mean significant wave height (H_s), energy period (T_e), and wave power (P), for the six buoys (B1–B6) shown in Fig. 1 for the period 2014–2016.

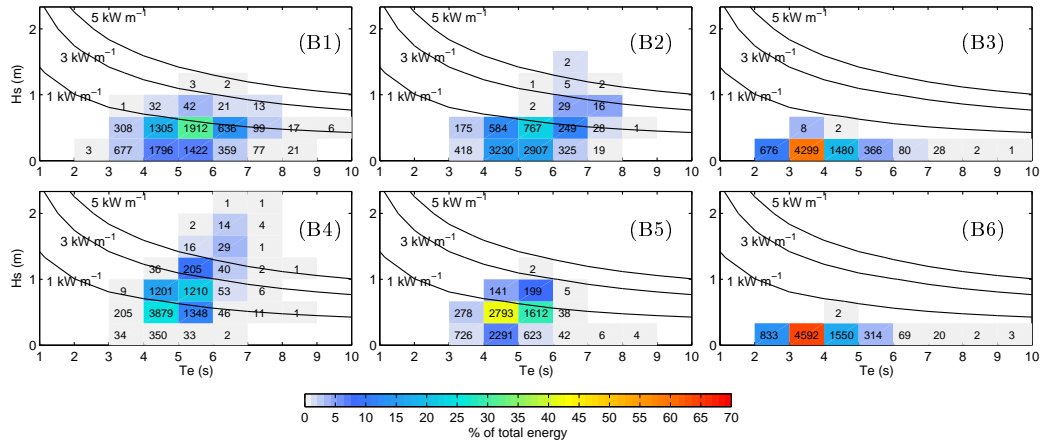


Figure 10: Bivariate distributions of occurrence and energy in terms of significant wave height (H_s), and energy period (T_e) averaged for the period 2014–2016 for at the six stations displayed in Fig. 1. The color scale, as a percentage, represents the contribution of the sea state to the total energy, while the black numbers indicates the occurrence of sea states in number of hours in one year.

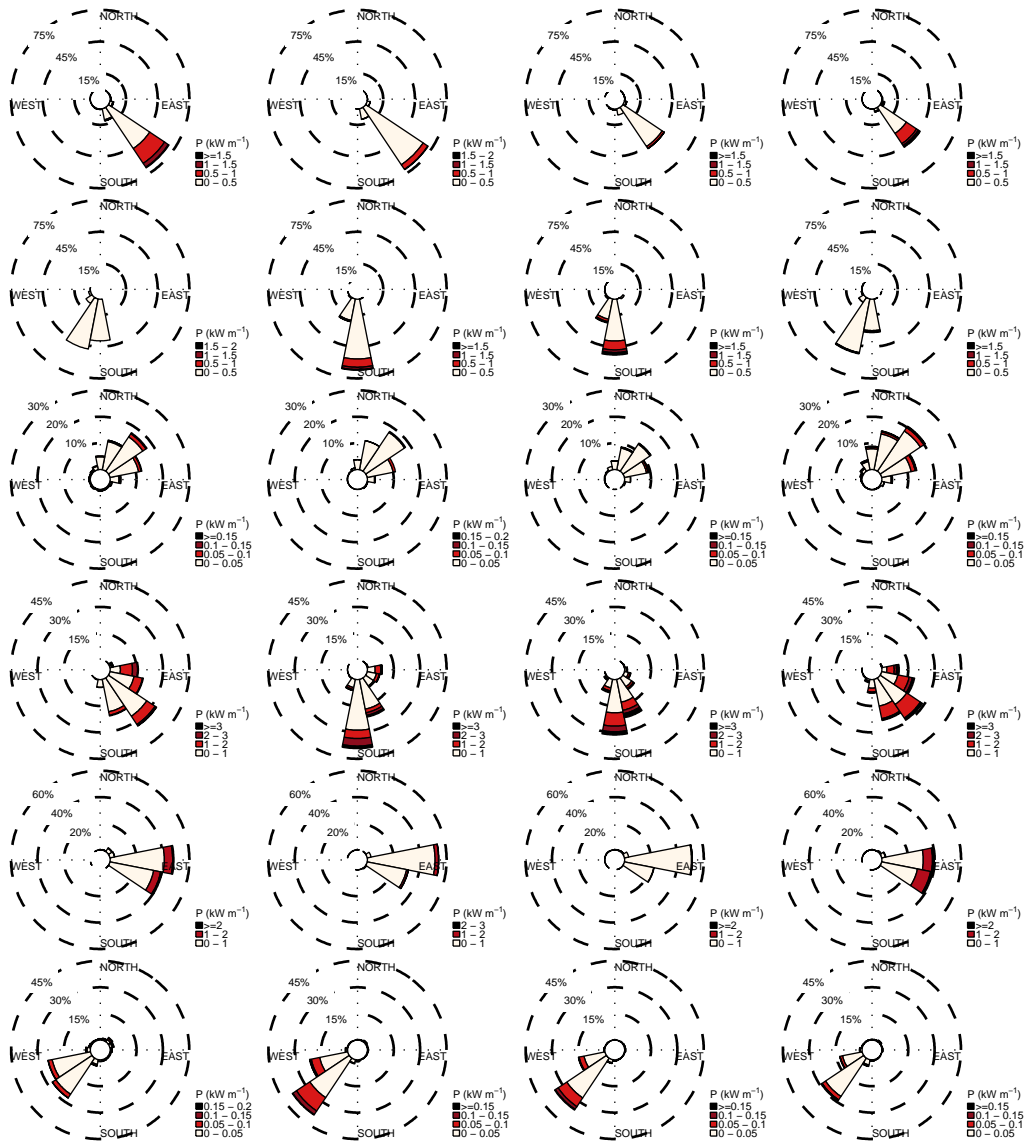


Figure 11: Seasonal wave power and direction roses based on the measurement from the buoys B1–B6 for the period 2014–2016.

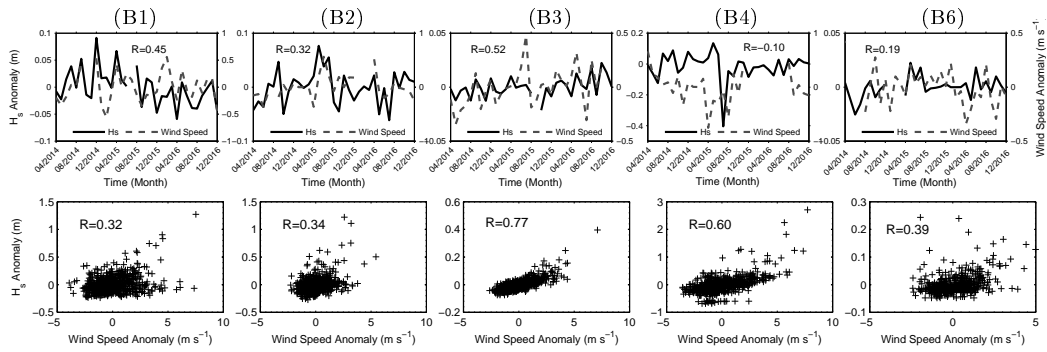


Figure 12: Top panel: the relationship between anomalies of monthly averaged data (monthly values minus monthly climatology) of wind speed and significant wave height, H_s , at buoys B1–B4 and B6 for the period 2014–2016. Bottom panel: the relationship between anomalies of daily averaged (daily values minus monthly climatology) of wind speed and H_s at the buoys B1–B4 and B6 (as above). R represents correlation coefficient.